communications physics

A Nature Portfolio journal

Article

https://doi.org/10.1038/s42005-025-02324-6

Entropy computing, a paradigm for optimization in open photonic systems

Lac Nguyen ✉, Mohammad-Ali Miri ✉, R. Joseph Rupert, Wesley Dyk, Sam Wu, Nick Vrahoretis, Irwin Huang, Milan Begliarbekov, Nicholas Chancellor, Uchenna Chukwu, Pranav Mahamuni, Cesar Martinez-Delgado, David Haycraft, Carrie Spear, Joel Russell Huffman, Yong Meng Sua & Yu-Ping Huang

Finding better solutions to combinatorial optimization problems could have a large positive impact on many real-world application areas, such as logistics. For this reason, significant efforts have been made to design novel optimization paradigms. Here we show an early instance of such paradigm in an optical setting, the entropy computing paradigm. Specifically, we experimentally demonstrate the feasibility of entropy computing by building a hybrid photonic-electronic computer that uses optical measurement and feedback to solve non-convex optimization problems. The system functions by using temporal photonic modes to create qudits in order to encode probability amplitudes in the time-frequency degree of freedom of a photon. This scheme, when coupled with with electronic interconnects, allows us to encode an arbitrary Hamiltonian into the system and solve non-convex continuous variables and combinatorial optimization problems. We show that the proposed entropy computing paradigm can act as a scalable and versatile platform for tackling a large range of NP-hard optimization problems.

In the domain of computational optimization, a significant number of problems are NP-hard, which is commonly considered the hardest class of optimization problems. It has been shown that there exists a polynomial-time mapping of all problems in NP[1,2] to a smaller set of complete problems, and further to their extension beyond decision problems, to NP-hard problems, including optimization. The computer science community largely believes that no polynomial-time algorithm exists for all problems in NP (as an efficient algorithm for any of these complete problems would imply), but this has yet to be proven. Finding high-quality approximations (or optimal solutions) in practical timescales is very important, since numerous real-world applications require solutions to NP-hard problems.

The inherently complex nature of such optimization problems necessitates the development of novel computational frameworks, both in terms of hardware and algorithms. Traditional computational methods implemented on Complementary Metal Oxide Semiconductor (CMOS) devices often struggle with the scale and complexity of these problems, leading to extended solution times or, in some cases, the inability to find an optimal solution within a reasonable time frame.

Various special purpose processors (both classical and quantum), such as analog solvers, have recently been proposed. A detailed review of some of these machines can be found in ref. 3. Many of the recently proposed classical special purpose processors are a class of CMOS devices, which effectively implement simulated annealing and related algorithms, a review of these devices can be found here[4,5].

Similarly, many quantum devices used for non-convex optimization are quantum annealers, which were first proposed by Kadowaki and Nishimori[6]. Quantum annealers differ from the more conventional gate-based quantum computing architectures, since they encode and solve problems via continuous time evolution. Recent theoretical investigations showed annealing-based architectures might give equivalent advantages to those seen in a gate model setting. Adiabatic quantum computing, an idealized setting of quantum annealing where very long anneal times are employed, was shown to give the same quadratic speedup[7] that Grover search yields in a gate-model device[8,9], and is the best that is achievable by any quantum algorithm[10]. Furthermore, a more general class of continuous-time algorithms can obtain the same speedup, including continuous-time quantum walks[11] and interpolations between adiabatic and quantum walk protocols[12]. Even more recently, the same advantage has also been shown to be possible through dissipative dynamics, similar to those that our device emulates[13]; similar effects can be used to solve optimization problems[14]. The physical realization of quantum annealers on superconducting platforms remains a challenge due to limitations on connectivity and scalability.

Numerous approaches have been made to make optical analog computers recently due to the advantage of light in energy efficiency, scalability,

Quantum Computing Inc (QCi), Hoboken, NJ, USA. ✉e-mail: lnguyen@quantumcomputinginc.com; amiri@quantumcomputinginc.com

and global connectivity[15]. A popular approach among all is coherent Ising machines (CIM)[16–18]. Superior time-to-convergence vs. problem size scaling compared to annealers was observed[19]. However, maintaining stable operation on CIM to avoid external perturbations, including amplitude heterogeneity or phase-stability demand over long fiber, is the main drawback that prevents this technology from being widely adopted[20,21].

It is important to note that CIM implementations solely focus on solving Ising-type problems. However, the landscape of computationally-hard optimization problems is not limited to Ising problems and contains, for example, binary, non-convex continuous-variable, integer, and mixed-integer problems. Many discrete NP-problems do not naturally or directly map to the Ising model's framework of binary spin states with quadratic interactions (although they must in a formal sense due to the definition of NP-hardness), and developing an effective mapping that accurately represents the original problem within the Ising framework can be highly non-trivial and is often achieved only with a high computational overhead. Work in this direction includes[22] where mappings for many problems were shown, mappings of maximum k-SAT problems for arbitrary k[23], mappings of the weighted maximum independent set problem and related problems[24]. Furthermore, incorporating constraints, which are often required in NP-hard problems, into the Ising model can increase the complexity of the problem formulation. This is typically accomplished by introducing additional spins (qubits in the context of quantum computing) and carefully designing the interaction terms to ensure that the constraints are properly enforced, which can significantly increase the size and complexity of the resulting Ising problem. An additional complication, particularly for analog computers, is that the ratio of the largest to the smallest relevant energy scales (the dynamic range) can be large in some problems, particularly when constraints are considered, or where mapping procedures to an incompatible hardware graph, for example, through minor embedding, must be performed[25]. The small dynamic range of any real hardware often limits the types of problems that can be efficiently solved on that hardware.

In light of these challenges, we present early steps toward a computing paradigm, *entropy computing*, that operates by conditioning a *quantum reservoir* to promote the stabilization of the ground state in an optical setting. In this approach, a target Hamiltonian is mapped onto an effective dissipative operator to solve an optimization problem in the photon number Hilbert space. This approach induces loss into the system to suppress the evolution of unwanted states while promoting the evolution of (qu)dits that represent lower energy states of the corresponding Hamiltonian. Here, we define entropy computing as a system that encodes information in photon number states with readout in the Fock basis, and employs a balance of loss and gain, potentially via measurement and feedback, to search for optimal solutions, following the principle of minimum entropy as discussed in ref. 26.

We experimentally demonstrate entropy computing through a hybrid optoelectronic measurement-feedback system that utilizes photon qudits encoded as probability amplitudes in time-frequency degree of freedom in conjunction with electronic interconnects for embedding an arbitrary Hamiltonian. In this manner, we demonstrate an entropy computing machine with a versatile polynomial loss function containing first- to fifth-order terms with fully programmable weight tensors, capable of solving optimization problems with up to 949 independent variables over a fixed summation constraint. We employ this platform for solving non-convex continuous variables and integer combinatorial optimization problems. While the goal of this paper is not to fully introduce the paradigm, we do include some discussion of how a more quantum version, which is still within this paradigm could be created in supplementary note 1.

Methods

Hybrid entropy computing system

In the first realization of this hardware, which is discussed here, we use time correlated single photon counting (TCSPC) and electro-optical feedback to emulate entropy computing, although for discounted computing power. We discuss in supplementary note 1 how an all-optical extension of this paradigm may be realized. The system configuration is illustrated in Fig. 1, where the loss mechanism is implemented through an electro-optical modulator (EOM) and the mixer is realized by passing the optical signals through a nonlinear optical circuit, detecting them in a single photon detector (SPD), and post-processing the TCSPC results. In details, the Hamiltonian problem is encoded into the amplitude of an electrical signal via digital-to-analog converter (DAC). The signal is used to drive an EOM device, which tailors a weak coherent state into single-photon signals in a shaped wave function, to realize high-dimensional time-bin encoding. The optical signal is then combined with and modulated by a coherent pump at a different wavelength as they pass through a quantum non-linear optical circuit. In this report, we use a periodically poled lithium niobate (PPNL) non-linear crystal as a sum frequency converter, where the signal light is a single-photon-level output from the EOM, and the pump photons are undepleted to ensure efficient conversion. At the output, the resultant single photons are detected by an SPD and recorded by a TCSPC. A clock signal is used as a reference where the period matches the feedback loop time. An FPGA accumulates photon counts of each time bin and computes the contribution of those counts to the losses of each time bin, thereby emulating the interaction terms in the Hamiltonian. Hence, the loss rate for each mode is the sum of a constant term, corresponding to the linear "chemical potential energy" of that mode, and a photon-number dependent term, corresponding to the nonlinear interaction energy. The quantum frequency converter, time-correlated single photon counter, SPD, and feedback through the EOM together act as the medium with linear and nonlinear losses. Single photon detection combined with FPGA normalization feedback promotes the least loss states in a hybrid framework. A secondary DAC embedded in the FPGA is used to continuously control variable optical attenuators (VOA), guaranteeing ultra-low mean photon number. While our entropy computing approach implementation is designed for photon number states or Fock states, it is practically difficult with the current state-of-the-art in deterministic photon number generation[27,28]. In the current hybrid implementation of Dirac-3, we use a common approximation of Fock states, which is coherent states with ultra-low mean photon number μ[29]. Dirac-3 is maintained such that about 1% or less of pulses have more than 1 photon. We further provide evidence that solution quality of Dirac-3 is affected by varying mean photon number.

In this system, the temporal bins form the state bases and TCSPC measures photon counts in each bin for stochastic computing with integer variables[30,31]. The weak coherent states with low power will approximately yield either vacuum or a superposition of single photons in each time bin, in other words states where two or more photons are present are exceedingly rare.

Figure 1c depicts measurements where one time bin is occupied after each measurement. Note that while we do often measure single photons, even very weak coherent states do not reproduce single photon statistics, for example, they would not be able to reproduce celebrated photon statistics effects, such as the Hong-Ou-Mandel effect[32,33]. They do, however, provide us with a convenient means to test early hybrid devices acting in the few-photon regime. Fluctuations are introduced through the shot noise of single-photon counting. Through the feedback, the photon counts of each time bin are used to condition the photon losses applied to the same or other time bins in the subsequent round-trip iteration. Hence, the quantum states evolve step-wise through a measurement-and-feedback setting. By enforcing a normalization condition for the total photons in all time bins, the photon numbers in each time bin will be incentivized to self-align into a configuration with the minimum loss, as the high-loss configurations will be "punished" through the loop iteration. As we can conveniently control the loss for individual time bins and the overall loss, one can apply constraints to photon numbers in each time bin or the sum of all. This gives the flexibility of optimizing practical problems that always come with various constraints.

Figure 1a presents a hybrid entropy computing system that operates on time-bin modes using a measurement-feedback scheme. The optical signal is generated by a C-band continuous-wave laser attenuated using a set of programmable VOAs to produce weak coherent states. This signal is then modulated by an EOM, driven by a radio-frequency (RF) waveform tailored

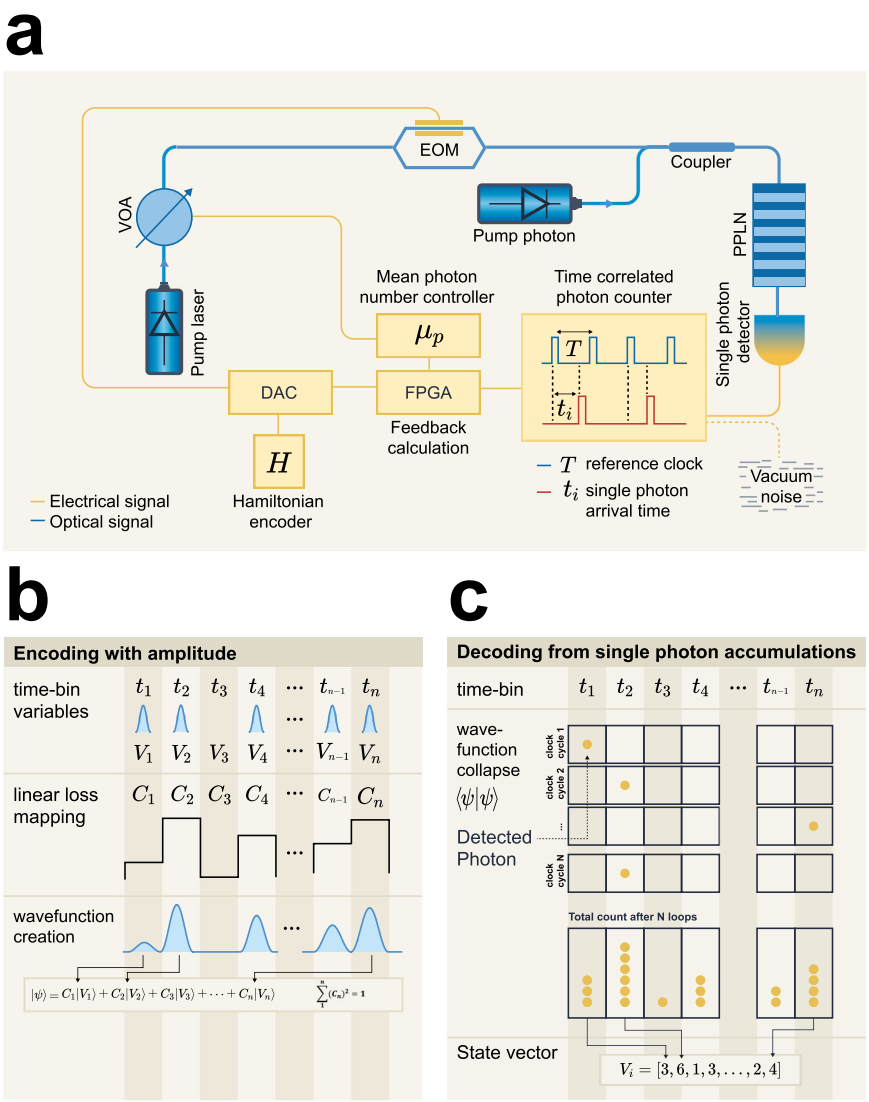

Fig. 1 | An emulation system for entropy computing using time-energy modes and a measurement-feedback scheme. a The optical signal is generated by a continuous-wave laser followed by a set of variable optical attenuators (VOA). It passes through the electo-optic modulator (EOM), the periodic-poled lithium niobate (PPLN) for nonlinear process, and is detected by a single photon detector (SPD). The time correlated single photon counting (TCSPC) results are fed to a field-programmable gate array (FPGA) board, where the radio-wave input to the EOM is calculated and generated in a digital-to-analog converter (DAC) for each time bin. Here, the nonlinear circuit (in this case sum frequency generation via PPLN), photon detector, and the FPGA function together as a mixer/encoder. **b** The quantum states are encoded into a train of time-bin states of light in the photon-number Hilbert space. The linear loss in the Hamiltonian is mapped into probability amplitudes of a wave function. Each variable of the objective function is assigned to each time bin, creating "qudit" equivalent that is widely used in high-dimensional temporal encoding in quantum random number generation, quantum key distribution, and single-photon sensing[62–64]. **c** The single photon collapsed states are collected one by one and accumulate to create the next feedback to tailor new wave functions in each loop. When the wave function evolutions reach a stable distribution, the number of photons collected in each bin are translated directly as a state vector multiplied with a normalization factor.

for each time bin. The modulated, single-photon-level signal is combined with an undepleted O-band pump in a periodically-poled lithium niobate (PPLN) waveguide for a sum-frequency generation (SFG) nonlinear process. The upconverted photons are detected using a high-efficiency, low-dark-count silicon single-photon detector (Si-SPD). Time-correlated single-photon counting (TCSPC) data is sent to a field-programmable gate array (FPGA), which computes the appropriate RF waveform and drives the EOM via a DAC on a per-time-bin basis. In this architecture, the nonlinear circuit (SFG in PPLN), photon detection, and FPGA together form a feedback-based optical mixer and encoder. Figure 1b, c show that, over multiple feedback loops, the accumulated photon counts in each time bin represent the values of corresponding variables. The resulting time-bin histograms at each iteration reflect the state vector of the Hamiltonian at that moment. For accurate operation, it is critical to maintain an ultra-low dark count rate in the SPD so that the measurement is dominated by shot noise. The speed of single-photon detection is a key factor influencing the overall feedback latency. To ensure a compact and stable system, PPLN is used to leverage the high efficiency and low dark count performance of the Si-SPD.

Coherent states quantum state of light closely resemble classical oscillations of the light field, but also include quantum noise, specifically shot noise. In this hybrid system, single photon count of each time-bin experience Poisson noise which is taken advantage as a source of "entropy" or "fluctuation", in each feedback loop. We define this parameter as "quantum fluctuation coefficient" that equals $\frac{1}{\sqrt{N}}$, following the standard deviation of Poisson distribution where N the number of photon collected in each time-bin. Therefore, throughout the measurement and feedback process, the injection of fluctuations enables a search of the solution space, which assists in bypassing the trapping of the system into local minima. The results section of this paper evidences that the solution quality of Dirac-3 is affected by varying quantum fluctuation or shot noise. We expect that an all optical system could perform even better and we discuss a route to one in supplementary note 1. It requires many incremental loops to find the global minimum solutions to optimization problems with many variables. It is worth noting that since the optical parts of the system do not involve large-scale non-Gaussian quantum superpositions, they could in principle be instead classically simulated, as has been argued in the coherent Ising machine setting[34,35]. In spite of this fact, these machines still provide a useful demonstration of what can be done in optical computing, and a preview of what a fully optical system may be able to do. The ultimate goal of a quantum version of an entropy computer would be to take full advantage of the non-Gaussian statistics induced by Fock-state measurement, this is discussed in supplementary note 4.

Dirac-3 optimization machine

The hybrid system can be used for a variety of optimization tasks, including those of binary variables, mixed-integer variables, quasi-continuous, and any combination of them. In this work, we focus on the minimization of the

following cost function E over variables v_i:

$$E = \sum_i C_i v_i + \sum_{i,j} J_{ij} v_i v_j + \sum_{i,j,k} T_{ijk} v_i v_j v_k + \sum_{i,j,k,l} Q_{ijkl} v_i v_j v_k v_l + \sum_{i,j,k,l,m} P_{ijklm} v_i v_j v_k v_l v_m . \quad (1)$$

Here, v_i ($i = 1, 2, 3, \cdots, N$) are real numbers over a discrete space, C_i are the linear terms' real-valued coefficients, while J_{ij}, T_{ijk}, Q_{ijkl}, P_{ijklm} represent two-body to fifth-body interaction coefficients that are real numbers subject to the tensors J, T, Q, and P being symmetric under all permutations of the indices. Furthermore, it is important to note that the probabilistic nature of the optimization variables in the proposed entropy computing method demands that all variables are non-negative, i.e., $v_i \geq 0$. To allow negative variables, a linear transformation of the variables needs to be applied prior to the problem encoding. While we are aware of proposals to implement higher-order interactions in similar optical settings (for example[36]), we are not aware of any other experimental implementations reported in the literature. It is also worth noting that we do not necessarily need dense higher-order interactions to encode interesting problems. As a concrete example, here, the hardest satisfiability problems occur when the number of clauses scales with the number of variables[37]. This concept seems to hold when quantum heuristics are considered as well[38].

In observation of the system openness due to effective dissipation and gain applied during each feedback loop, a constraint on the sum of the variables v_i can be applied such that:

$$\sum_i v_i = R. \quad (2)$$

Thus, the proposed scheme finds minimal solutions of the loss function of Eq. (1) subject to the sum constraint of Eq. (2).

Given a desired optimization problem formulated in the form of relation (1), the optimization process is described below. First, a sum constraint R is chosen. Clearly, without a knowledge of the final solution, the true sum of variables $\sum_i v_i$ is unknown. But one can readily bypass this problem by introducing slack variables, as discussed in an example in the next section. Once the sum is predetermined, an initial photon qudit state is generated from the noise and launched in the system. After propagating in the closed loop, the photonic state is measured and evaluated to prepare the state for the next iteration.

In stark contrast with the Ising Hamiltonian, which is the basis model for the majority of quantum annealers, the above objective function involves polynomial terms (up to fifth order in our present experimental demonstration) over discretized variables. In this regard, the proposed hybrid quantum optimization machine offers two immediate advantages over an Ising solver; (i) it can naturally represent higher than binary optimization problems, and (ii) it involves k-body interaction terms ($k = 1, 2, 3, 4, 5$). Accordingly, it offers great potential in efficiently solving continuous and integer variables as well as problems that naturally involve higher-order interaction terms, such as the satisfiability boolean, without requiring additional complex encoding or incorporating auxiliary variables that add to the size of the problem in case of an Ising solver. Furthermore, the proposed machine naturally allows for dense long-range interactions in all orders of the interactions, which alleviates the requirement for complex embedding algorithms. Here, we report results from our first commercially available machine, which we call Dirac-3. Dirac-3 is an optimization solver that implements the entropy computing paradigm discussed above.

Results

In the following, we first use a simple 2-variable problem to illustrate the optimization process in our early hybrid implementation of our entropy computing paradigm. Next, we present results from two benchmark hard optimization problems from known libraries. In general, benchmarking systems like ours is a challenging problem. We do, however, present some promising experiments to show how the technology works. Here, we use two different types of problems: a non-convex quadratic problem and a combinatorial graph cut problem.

We first consider a simple two-variable optimization problem, defined through the objective function $g(x, y) = (x^4 + y^4)/4 - 5(x^3 + y^3)/3 + 3(x^2 + y^2)$. As depicted in Fig. 2a, this function contains three local minima at (x, y) = {(0, 3), (3, 0), (3, 3)} as well as a global minimum at (x, y) = (0, 0). To solve this problem using Dirac-3, we consider 3 variables v_1, v_2, and v_3, with v_1 and v_2 representing x and y, respectively, while v_3 represents a slack variable, which is not coupled to any other variable but used to effectively relax the sum constraint. In this manner, one can consider a relatively large sum constraint of $R = 100$ to incorporate a larger range of potential solutions. Figure 2b shows the evolution of the energy level for 20 different runs as the system evolves toward an equilibrium point. The evolution of the variables versus the number of iterations is shown in Fig. 2c for three exemplary cases. These figures indicate rapid convergence of the solution after only a few iterations. Even more interestingly, the trajectories of the optimization variables in the two-dimensional (x, y) plane (Fig. 2d–k) show that the system takes steps to avoid the local minima, even though in all cases the initial point was located within the attractor basins of the local minima.

We next consider a non-convex quadratic optimization problem (QPLIB_0018) with 50 continuous variables over a fully connected weighted graph, selected from QPLIB, a library of quadratic programming instances[39]. The cost function of this problem is of the form $f(\mathbf{x}) = C^T\mathbf{x} + \mathbf{x}^T J\mathbf{x}$, where, $\mathbf{x} = (x_1, x_2, \cdots, x_{50})^T$ and $x_i \geq 0$. Figure 3a show the equilibrium energy distribution over 500 runs of Dirac-3 compared with the results obtained from a conventional gradient descent algorithm. Dirac-3 successfully finds the ground state in almost 80% of instances. The evolution of the energy level is plotted as a function of the iterations (red) and compared with those obtained from gradient descent (blue) over 50 different runs, shown in Fig. 3c. The inset depicts the evolution of the solution with the number of iterations, indicating rapid convergence of the solution after a few iterations. An important observation here is that the problem is hard enough for gradient descent to become stuck in a sub-optimal solution, but that Dirac is able to avoid these local minima and find the true optima. This shows that the device is able to do more than just perform updates based on local information from flipping single bits, an encouraging sign for the method.

It is important to evaluate the performance of the entropy computing machine while operating with classical versus quantum states of light. We currently use (weak) coherent states as input, while weak coherent states by themselves always behave classically regardless of average photon number, interactions with nonlinear elements can yield quantum states within the device itself; therefore, discussion of quantum states is justified. However, very strong nonlinearity (stronger than is currently available) would be needed to be able to achieve all optical implementation, see discussion in supplementary note 1. For this purpose, we investigate the optimization performance for various mean photon numbers μ_p associated with both regimes. As the same time, we explore how solution quality is affected when shot noise is varied in each feedback loop. It is expected that a high probability of operating in the single-photon regime and high shot noise are required in every feedback loop to constantly boost the stochasticity of the system, promoting chances of jumping out of local minima.

We perform the experiment using the same non-convex quadratic optimization problem (QPLIB_0018) from the library for programming instances. In the current Dirac-3, we varied μ_p from 0.03 to 1.33% which is equivalent to 98.67 to 99.97% probability of a single-photon regime. Note that similar strategies, but not at such extremely low photon numbers have shown promise in CIM[40]. Figure 3b shows the average energy level returns after 20 runs versus the various mean photon number and quantum fluctuation coefficient. Each pixel represents the average energy returns (Fig. 3b) after 20 runs. Thus, this experiment provides evidence that better solutions or lower average energy returns for an optimal range are associated with lower mean photon numbers. By increasing μ_p the solution quality deteriorates as the system is more likely to be trapped in local minima. On the

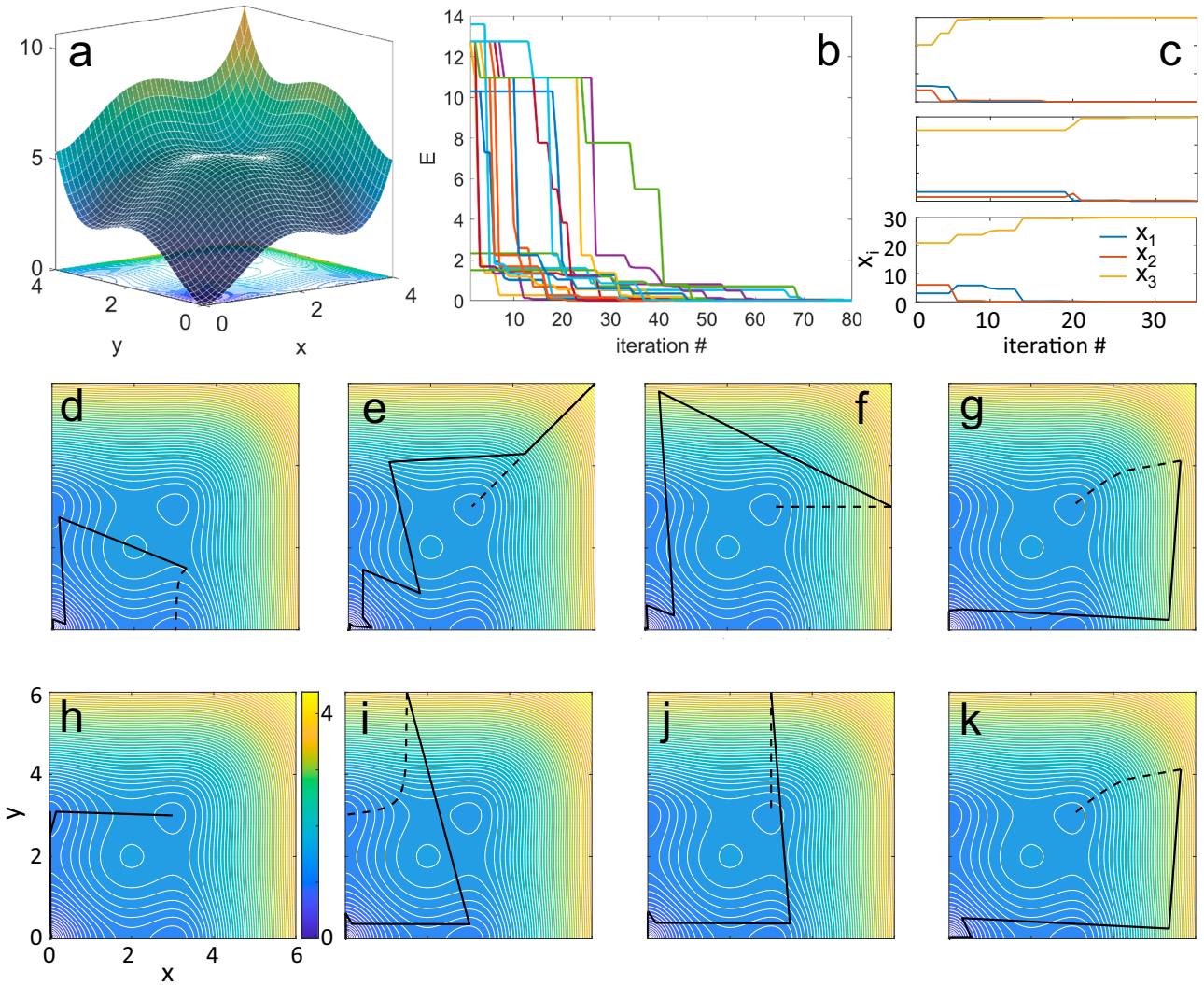

Fig. 2 | Solving a two-variable non-convex quadratic optimization problem. A two-variable non-convex polynomial optimization problem is considered. **a** A visualization of the energy landscape that involves three local minima and a global minimum at (x, y) = (0, 0). **b** The iterative evolution of the cost function of the proposed hybrid entropy computing solver over 20 runs. **c** Three exemplary evolutions of the optimization variables involved, including the slack variable (x_3), over iterations of the entropy computing solver. **d–k** Eight exemplary trajectories of the optimization variables in the two-dimensional (x, y) plane as the solver evolves toward equilibrium while starting from different initial conditions. In these figures, the solid lines show the trajectory of the entropy-computing solver, while the dashed lines depict the trajectory of a gradient-descent solver. More details on the gradient descent method can be found in supplementary note 3.

other hand, lower μ_p promotes more single photon states, leading to higher probabilities of escaping local minima and converging to the global minimum. Furthermore, it is important to note that there is a trade-off between increasing the quality of the solution by operating in the low-photon-number regime and reducing the optimization time. Operating at lower photon numbers requires a longer time to accumulate enough photons, leading to an increase in time for the system to stabilize in an equilibrium state. Notice that further reducing the single photon rate, the classical (thermal) noise from the single-photon detector's dark count deteriorates the results, too. This can be quantified into a parameter, the quantum-to-classical ratio (QCR), defined as the photon detection rate divided by the dark count rate, which decreases for lower photon numbers. Fig. 3d, e captures the number of ground states found after 500 runs when decreasing μ_p (from right to left) when optimizing QPLIB_18 problem, ground states are found more often. However, when the average photon count reaches the dark count level of the SDP, the number of ground states found reduces accordingly.

Solution quality evidently changes while studied with various quantum fluctuation coefficients. Values of the vertical axis on Fig. 3d shows the percentage of shot noise present when collecting photons in each time bin. For example, 0.1 quantum coefficient fluctuation means 10% of the photon count measured across all time bins comes from Poisson noise. In this experiment, increasing shot noise (top to bottom) shows improvement in average returned energy over multiple runs. This also explains the evolution trajectory of Dirac-3 in searching for optimal solution in a non-convex energy landscape shows "quantum-tunneling-like" behavior in Fig. 2. As the system appears to be able to escape local minima highly effectively. Notice that true tunneling would require a large-scale quantum superposition, which is not realizable in a hybrid setting. However, numerous classical systems can illustrate behavior that is similar to tunneling and matches tunneling rates. This can be seen in ref. 41 through the physics of a semi-classical diabatic cascade, or in the ability of path-integral quantum Monte Carlo (a classical algorithm) to match the tunneling rates through a simple barrier[42].

In this hybrid optimization machine implementation, FPGA can be conveniently engineered to accommodate these higher order of interaction terms, making this architecture practical with current technology[43,44]. Thus, on this hybrid measurement-feedback-based approach, time-to-convergence depends partially on the FPGA and its architecture for the multiplier. It is worth emphasizing that this current FPGA-feedback-based

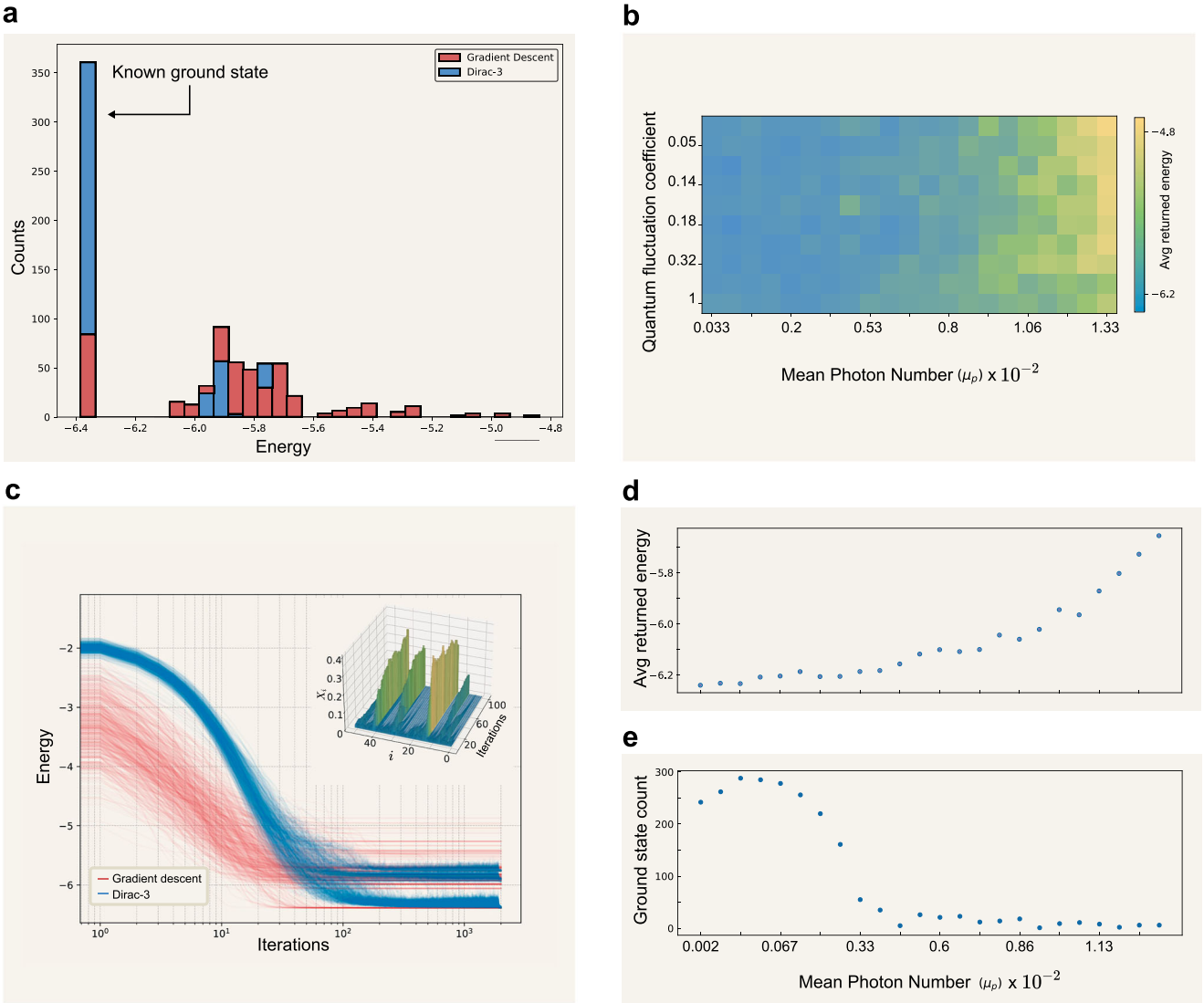

Fig. 3 | Solving a non-convex continuous optimization problem. A non-convex quadratic optimization problem with 50 variables is considered (QPLIB_0018). **a** Energy distribution over 500 runs of Dirac-3 (blue) and gradient descent algorithm (red). **c** Energy evolution versus the number of iterations on Dirac-3 (blue) and gradient descent (red). The inset shows the evolution of the solution versus iterations. **b** Relationship between the mean photon number (μ), quantum fluctuation coefficient,and key performance metrics - average returned energy. The transition from left to right represents an increase in mean photon number (μ), showing the probability that Dirac-3 is operating in a single-photon regime. Quantum fluctuation or shot noise is used as $\frac{1}{\sqrt{N}}$ where N is the number of photon count accumulated in each time-bin. From the bottom to the top of the vertical axis, this coefficient is gradually decreased. **d**,**e** Average returned energy and number of ground states found after 500 runs are collected when mean photon number is decreased further up to 0.002%, close to the level of dark count of single photon detector.

architecture cannot support large-scale quantum superpositions, similar to measurement-and-feedback-based CIM[45]. However, such an early implementation can provide an test of how the algorithms can perform even in the absence of such correlations, being able to perform well in this setting is valuable evidence for how well an eventual device based on optical interference could preform. While the use of the FPGA is a key limitation, we believe that relatively early (in the implementation of the paradigm) tests, such as those performed here, provide an important indication as to whether the direction is viable to support highly performant optimization. In this case, the results are suggestive that it indeed can.

Next, we consider a combinatorial optimization problem, the maximum cut (max-cut) problem, that is known to be NP-hard. Considering for simplicity an unweighted graph, the max-cut is a partition of its vertices into two complementary sets, such that the number of edges between the two sets is maximal. This problem can be generalized to maximum k-cut (max-k-cut), where, the vertices are partitioned into k disjoint subsets, such that the number of edges between the k subsets is maximized. Although the proposed entropy computing paradigm deals with continuous-valued variables in general, it can be utilized to solve such discrete problems by suitable encoding of a discrete (e.g., spin) degree of freedom in the continuum, which can be done in different ways. One way is to map a binary variable $s_i \in \{0, 1\}$ onto a vector $\vec{\mathbf{s}}_i = x_i \begin{pmatrix} 1 \\ 0 \end{pmatrix} + y_i \begin{pmatrix} 0 \\ 1 \end{pmatrix}$. In this manner, one can embed a classical bit onto the continuum and identify the two states by taking the maximum of x_i and y_i variables. Furthermore, the values of x_i and y_i can be regularized by considering a regularization term that can be chosen as $x_i + y_i = 1$ in its simplest way. This approach can be readily extended to consider a ternary digit (trit), a quaternary digit (quit), and so on, which allows for tackling a general k-state standard Potts problem with the proposed entropy computing machine.

Now, considering a graph with N nodes, described with adjacency matrix A, i.e., $A_{ij} = 1$ for adjacent nodes and $A_{ij} = 0$ otherwise, the max-k-cut problem can be formulated as minimizing the following objective function: $E = \sum_{i,j} A_{ij} \vec{\mathbf{s}}_i \cdot \vec{\mathbf{s}}_j + \lambda \sum_i \left\| \vec{\mathbf{s}}_i - \mathbf{1} \right\|_1^2$, where the second term is an

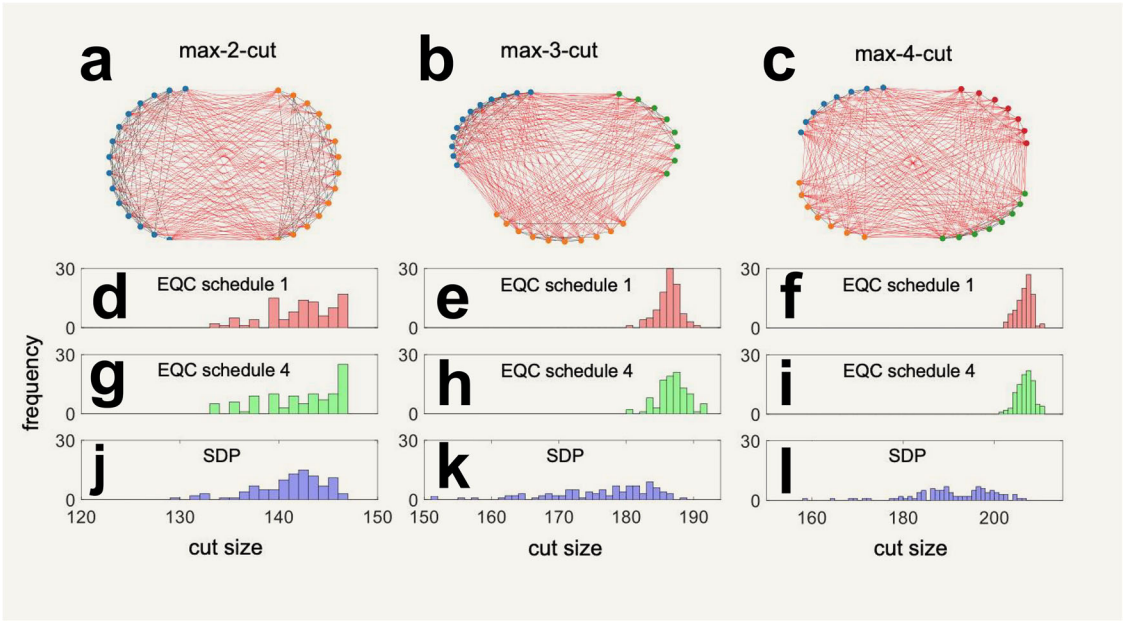

Fig. 4 | The results for solving the max-k-cut problem. The optimization results for solving combinatorial problems of max-cut, max-3-cut, and max-4-cut on a 30-node unweighted graph that is generated randomly with $p = 0.5$ probability of connectivity between each two nodes. **a–c** The visualizations of exemplary graph cuts with different numbers of partitions. **d–f** The distribution of the cut sizes over 100 runs of the max-2-cut (traditional max-cut), max-3-cut, and max-4-cut problems on Dirac-3 using relaxation schedule 1. **g–i** Similar distributions when using the schedule 4. **j–l** The distribution of the cut sizes over 100 runs of the same problems using semi-definite programming (SDP).

L1-norm regularization term with a parameter λ. It is straightforward to cast this objective function in the form of relation (1). This results in a quadratic function involving qN variable, where q is the dimension of a single artificial spin state and N is the size of the graph.

To test this formulation, we consider a randomly generated graph of $N = 30$ nodes such that each two nodes are connected with a probability of $p = 0.5$. Figure 4a–c visualizes exemplary partitioning of this graph into 2, 3, and 4 groups through the proposed entropy computing system. This particular graph has 233 total links, and we found the maximum cut size to be 146. Histograms of the cut sizes obtained for 100 different runs of the max-cut, max-3-cut, and max-4-cut problems using the entropy computing solver at schedule 1 are shown in Fig. 4d–f, and using schedule 4 in Fig. 4g–i. The results are compared with those obtained from Semi-Definite Programming (SDP) shown in Fig. 4j–l. Here, we used the CVXPY package with the SCS solver to solve the semidefinite program. As expected, we observe that schedule 4 provides better results. In the version of Dirac-3 reported here, schedule 1 was set to have a smaller number of feedback loops, a lower quantum fluctuation coefficient, and a higher mean photon number compared to schedule 4. In addition, as this figure clearly indicates, in all cases the entropy computing machine provides excellent results that outperform SDP results. As a reference, it is worth mentioning that SDP relaxation for max-cut has a performance guarantee of the ratio of 0.878[46], which translates to a cut size of 128 for the particular graph considered here. For the results presented in Fig. 4, the regularization parameter was chosen to be $\lambda = 5$.

Discussion

We experimentally demonstrated entropy computing through a hybrid photonic-electronic system that builds on time-multiplexed photon qudit time bins propagating in a closed feedback loop involving electronic interconnects for implementing a reconfigurable effective optimization cost function. We demonstrated the successful operation of the proposed system for solving non-convex and combinatorial optimization problems. Results show that Dirac-3 found the ground state more often than classical gradient descent on a non-convex optimization problem with constraints. Dirac-3 also performs superior to SDP in solution quality on Ising and standard Potts problems. The presence of the sum constraint in the current Dirac-3 machine becomes an advantage in problems that intrinsically involve this natural restriction. Such problems emerge in portfolio optimization, resource allocation problems, diet problems, knapsack, network flow problems, and election and voting systems[47–50]. One of the key strengths of the proposed entropy computing machine is its flexibility in encoding, allowing it to handle continuous and integer variables. This capability sets it apart from many classical and quantum solvers that are primarily designed for binary Ising/QUBO problems, and it opens up new possibilities for efficient solutions in diverse applications, including grid optimization and machine learning tasks like clustering and decomposition[51,52]. Traditionally, implementing higher-order interactions in Ising, Potts, or XY problems on analog hardware solvers requires a quadratization step for polynomial reduction[23,53,54]. Dirac-3 simplifies this process by directly mapping high-order optimization problems, promising an increase in precision and solution quality while consuming fewer resources by eliminating the need for auxiliary variables[55,56]. Further studies and benchmarking are necessary to fully explore the capabilities of Dirac-3.

The speed of our approach comes from the relaxation mechanism as well as the fast propagation and processing of information within light. Our current Dirac-3 hybrid implementation does not utilize quantum entanglement. Rather, we demonstrated that our approach to analog optimization is capable of escaping local minima in dense NP-hard problems and performs well, using the intrinsic randomness of quantum fluctuations in photon number, an early demonstration of a key aspect of our paradigm of entropy computing. Recently, some studies have demonstrated that taking advantage of quantum superposition, which extends from the double-slit experiment, key role to discovery of quantum mechanics, provides advantage in computation, machine learning, and imaging tasks[57–59].

The current hybrid architecture of the entropy computing system exhibits low energy consumption (below 100 W during operation), comparable to a laptop. Further benchmarking needs to be done to appreciate energy advantages of this architecture. This energy footprint is expected to decrease significantly when the system is implemented entirely on an integrated photonic platform. This shift towards an all-optical approach holds promise for a practical and sustainable unconventional computing

paradigm, contributing to solving energy rising issues by high performance computing[60,61].

Data availability

Data associated with this paper can be found at https://github.com/qci-github/eqc-studies/blob/main/eqc-paradigm/eqc_vs_grad/grad_vs_eqc.py. The same data are available on a figshare repository at https://doi.org/10.6084/m9.figshare.29949722.

Code availability

Code associated with this paper can be found at https://github.com/qci-github/eqc-studies/blob/main/eqc-paradigm/eqc_vs_grad/grad_vs_eqc.py. The same code is available on a figshare repository at https://doi.org/10.6084/m9.figshare.29949722.

Received: 19 March 2025; Accepted: 22 September 2025;
Published online: 24 October 2025

References

1. Cook, S. A. The complexity of theorem-proving procedures. In *Proc. Third Annual ACM Symposium on Theory of Computing*, STOC '71, 151–158 (Association for Computing Machinery, 1971).
2. Karp, R. M.*Reducibility among Combinatorial Problems*, 85–103 (Springer, 1972).
3. Mohseni, N., McMahon, P. L. & Byrnes, T. Ising machines as hardware solvers of combinatorial optimization problems. *Nat. Rev. Phys.* **4**, 363–379 (2022).
4. Matsubara, S. et al. Digital annealer for high-speed solving of combinatorial optimization problems and its applications. In *2020 25th Asia and South Pacific Design Automation Conference (ASP-DAC)*, 667–672 (ASP-DAC, 2020).
5. Kao, Y.-T., Liao, J.-L. & Hsu, H.-C. Solving combinatorial optimization problems on fujitsu digital annealer ArXiv:2311.05196 (2023).
6. Kadowaki, T. & Nishimori, H. Quantum annealing in the transverse Ising model. *Phys. Rev. E* **58**, 5355–5363 (1998).
7. Roland, J. & Cerf, N. J. Quantum search by local adiabatic evolution. *Phys. Rev. A.* **65**, 042308 (2002).
8. Grover, L. K. A fast quantum mechanical algorithm for database search. In *Proc. Twenty-Eighth Annual ACM Symposium on Theory of Computing*, STOC '96, 212–219, https://doi.org/10.1145/237814.237866 (Association for Computing Machinery, 1996).
9. Grover, L. K. Quantum mechanics helps in searching for a needle in a haystack. *Phys. Rev. Lett.* **79**, 325–328 (1997).
10. Bennett, C. H., Bernstein, E., Brassard, G. & Vazirani, U. Strengths and weaknesses of quantum computing. *SIAM J. Comput.* **26**, 1510–1523 (1997).
11. Childs, A. M. & Goldstone, J. Spatial search by quantum walk. *Phys. Rev. A* **70**, 022314 (2004).
12. Morley, J. G., Chancellor, N., Bose, S. & Kendon, V. Quantum search with hybrid adiabatic–quantum-walk algorithms and realistic noise. *Phys. Rev. A* **99**, 022339 (2019).
13. Berwald, J., Chancellor, N. & Dridi, R. Grover speedup from many forms of the Zeno effect. *Quantum* **8**, 1532 (2024).
14. Berwald, J., Chancellor, N. & Dridi, R. Zeno-effect computation: opportunities and challenges. *Phys. Rev. A* **111**, 042623– (2025).
15. Stroev, N. & Berloff, N. G. Analog photonics computing for information processing, inference, and optimization. *Adv. Quantum Technol.* **6**, 2300055 (2023).
16. Yamamoto, Y. et al. Coherent ising machines—optical neural networks operating at the quantum limit. *npj Quantum Inf.* **3**, 49 (2017).
17. Yamamoto, Y., Leleu, T., Ganguli, S. & Mabuchi, H. Coherent Ising machines-quantum optics and neural network perspectives. *Appl. Phys. Lett.* **117**, 160501 (2020).
18. McMahon, P. L. et al. A fully programmable 100-spin coherent Ising machine with all-to-all connections. *Science* **354**, 614–617 (2016).
19. Hamerly, R. et al. Experimental investigation of performance differences between coherent Ising machines and a quantum annealer. *Sci. Adv.* **5**, eaau0823 (2019).
20. Leleu, T., Yamamoto, Y., McMahon, P. L. & Aihara, K. Destabilization of local minima in analog spin systems by correction of amplitude heterogeneity. *Phys. Rev. Lett.* **122**, 040607 (2019).
21. Wang, Z., Marandi, A., Wen, K., Byer, R. L. & Yamamoto, Y. Coherent ising machine based on degenerate optical parametric oscillators. *Phys. Rev. A* **88**, 063853 (2013).
22. Lucas, A. Ising formulations of many NP problems. *Front. Phys.* **2**, 5 (2014).
23. Chancellor, N., Zohren, S., Warburton, P. A., Benjamin, S. C. & Roberts, S. A direct mapping of max k-sat and high order parity checks to a chimera graph. *Sci. Rep.* **6**, 37107 (2016).
24. Choi, V. Adiabatic quantum algorithms for the NP-complete maximum-weight independent set, exact cover and 3sat problems, https://arxiv.org/abs/1004.2226 1004.2226 (2010).
25. Choi, V. Minor-embedding in adiabatic quantum computation: I. The parameter setting problem. *Quantum Information Processing* 193–209 arXiv:0804.4884 (2008).
26. Vadlamani, S. K., Xiao, T. P. & Yablonovitch, E. Physics successfully implements Lagrange multiplier optimization. *Proc. Natl. Acad. Sci. USA* **117**, 26639–26650 (2020).
27. Uria, M., Solano, P. & Hermann-Avigliano, C. Deterministic generation of large Fock states. *Phys. Rev. Lett.* **125**, 093603 (2020).
28. Ma, Y.-X. & Li, P.-B. Deterministic generation of phononic Fock states via weak nonlinearities. *Phys. Rev. A* **108**, 053709 (2023).
29. Gisin, N., Ribordy, G., Tittel, W. & Zbinden, H. Quantum cryptography. *Rev. Mod. Phys.* **74**, 145–195 (2002).
30. Bouchard, F., England, D., Bustard, P. J., Heshami, K. & Sussman, B. Quantum communication with ultrafast time-bin qubits. *PRX Quantum* **3**, 010332 (2022).
31. Kaiser, J. & Datta, S. Probabilistic computing with p-bits. *Appl. Phys. Lett.* **119**, 150503 (2021).
32. Hong, C. K., Ou, Z. Y. & Mandel, L. Measurement of subpicosecond time intervals between two photons by interference. *Phys. Rev. Lett.* **59**, 2044–2046 (1987).
33. Gerry, C. & Knight, P. *Introductory Quantum Optics* (Cambridge University Press, 2004).
34. Clements, W. R. et al. Gaussian optical ising machines. *Phys. Rev. A* **96**, 043850 (2017).
35. Tiunov, E. S., Ulanov, A. E. & Lvovsky, A. I. Annealing by simulating the coherent Ising machine. *Opt. Express* **27**, 10288–10295 (2019).
36. Bashar, M. K. & Shukla, N. Designing Ising machines with higher order spin interactions and their application in solving combinatorial optimization. *Sci. Rep.* **13**, 9558 (2023).
37. Selman, B., Mitchell, D. G. & Levesque, H. J. Generating hard satisfiability problems. *Artif. Intell.* **81**, 17–29 (1996).
38. Santra, S., Quiroz, G., Ver Steeg, G. & Lidar, D. A. Max 2-sat with up to 108 qubits. *N. J. Phys.* **16**, 045006 (2014).
39. Furini, F. et al. QPLIB: a library of quadratic programming instances. *Math. Program. Comput.* **11**, 237–265 (2019).
40. Kumagai, M. et al. Single photon coherent Ising machines for constrained optimization problems. *Quantum Sci. Technol.* **10**, 035042 (2025).
41. Muthukrishnan, S., Albash, T. & Lidar, D. A. Tunneling and speedup in quantum optimization for permutation-symmetric problems. *Phys. Rev. X* **6**, 031010 (2016).
42. Isakov, S. V. et al. Understanding quantum tunneling through quantum Monte Carlo simulations. *Phys. Rev. Lett.* **117**, 180402 (2016).
43. Dou, Y., Vassiliadis, S., Kuzmanov, G. K. & Gaydadjiev, G. 64-bit floating-point FPGA matrix multiplication. In *Symposium on Field Programmable Gate Arrays,*https://api.semanticscholar.org/CorpusID:17013227 (2005).

44. Noble, G., Nalesh, S., Kala, S. & Kumar, A. Configurable sparse matrix-matrix multiplication accelerator on FPGA: A systematic design space exploration approach with quantization effects. *Alex. Eng. J.* **91**, 84–94 (2024).
45. Motta, M. et al. Determining eigenstates and thermal states on a quantum computer using quantum imaginary time evolution. *Nat. Phys.* **16**, 205–210 (2020).
46. Goemans, M. X. & Williamson, D. P. Improved approximation algorithms for maximum cut and satisfiability problems using semidefinite programming. *J. ACM (JACM)* **42**, 1115–1145 (1995).
47. Ajagekar, A., Hamoud, K. A. & You, F. Hybrid classical-quantum optimization techniques for solving mixed-integer programming problems in production scheduling. *IEEE Trans. Quantum Eng.* **3**, 1–16 (2022).
48. Ji, Y., Chen, X., Polian, I. & Ban, Y. Algorithm-oriented qubit mapping for variational quantum algorithms. *Phys. Rev. Appl.* **23**, 034022 (2024).
49. Witt, A., Kim, J., Körber, C. & Luu, T. ILP-based resource optimization realized by quantum annealing for optical wide-area communication networks – a framework for solving combinatorial problems of a real-world application by quantum annealing. *Front. Sci. Comput.* **10**, 1356983 (2024).
50. Neukart, F. et al. Traffic flow optimization using a quantum annealer. *Front. ICT* **4**, 29 (2017).
51. Hua, C., Rabusseau, G. & Tang, J. High-order pooling for graph neural networks with tensor decomposition. *Neural Inf. Process. Syst.* **436**, 6021–6033 (2022).
52. Kumar, V., Bass, G., Tomlin, C. & Dulny, J. Quantum annealing for combinatorial clustering. *Quantum Inf. Process.* **17**, 39 (2018).
53. Chancellor, N. Domain wall encoding of discrete variables for quantum annealing and QAOA. *Quantum Sci. Technol.* **4**, 045004 (2019).
54. Chang, C. C., Chen, C.-C., Koerber, C., Humble, T. S. & Ostrowski, J. Integer programming from quantum annealing and open quantum systems 2009.11970 (2020).
55. Bybee, C. et al. Efficient optimization with higher-order Ising machines. *Nat. Commun.* **14**, 6033 (2023).
56. Sharma, A. et al. Augmenting an electronic ising machine to effectively solve Boolean satisfiability. *Sci. Rep.* **13**, 22858 (2023).
57. Li, L., Kumar, S., Garikapati, M. & Huang, Y.-P. First photon machine learning, https://api.semanticscholar.org/CorpusID:273532446 (2024).
58. Taddei, M. M. et al. Computational advantage from the quantum superposition of multiple temporal orders of photonic gates. *PRX Quantum* **2**, 010320 (2021).
59. Zhang, H., Kumar, S. & Huang, Y.-P. Super-resolution optical classifier with high photon efficiency. *Opt. Lett.* **45**, 4968–4971 (2020).
60. Electricity 2024, Analysis and Forcast to 2026. Tech. Rep., International Energy Agency, Paris https://www.iea.org/reports/electricity-2024 (2024).
61. Andrae, A. & Elder, T. On global electricity usage of communication technology: trends to 2030. Tech. Rep (2015).
62. Rehain, P. et al. Single-photon vibrometry. *Opt. Lett.* **46**, 4346–4349 (2021).
63. Nguyen, L., Rehain, P., Sua, Y. M. & Huang, Y.-P. Programmable quantum random number generator without postprocessing. *Opt. Lett.* **43**, 631–634 (2018).
64. Mower, J. et al. High-dimensional quantum key distribution using dispersive optics. *Phys. Rev. A* **87**, 062322 (2013).

Acknowledgements

The authors would like to thank other scientists at Quantum Computing Inc including Prajnesh Kumar, Jeevanandha Ramanathan, and Malvika Garikapati for their valuable engineering suggestions. NC was fully supported by QCi in performing this work, in particular no UKRI support was received for writing this paper. The authors thank Mark Campanelli for providing software support for the execution of these experiments.

Author contributions

Y.H. conceived the concept of the hybrid entropy computing hardware. L.N. designed and built the computing hardware. Y.M.S., R.J.R., S.W., N.V., P.M., C.M.-D., D.H., and C.S. contributed to the development, construction, and testing of the computing hardware. D.H. and L.N. designed the experiments to characterize the system and interpreted the results. M.-A.M., W.D., and I.H. conceived and designed the problems and algorithms used to study the computing hardware. M.-A.M., N.C., L.N., Y.H., and M.B. drafted the manuscript. R.H. contributed to visualization by designing and producing images, diagrams, and graphical representations of the concepts and results. N.C., M.-A.M., and U.C. revised, organized, and finalized the manuscript.

Competing interests

All authors hold shares or options in QCi. Y. Huang is named on a related patent: “Super Ising emulator with multi-body interactions and all-to-all connections” which has numbers US20230185160A1 (USA), WO2021231794A1 (worldwide), JP2022569453A (Japan), EP4150430A1 (Europe), KR20230011342A (South Korea), CA3178484A1 (Canada), CN115698897A (China). Y. Huang is in the process of applying for an additional process related to underlying technology.

Additional information

Supplementary information The online version contains supplementary material available at https://doi.org/10.1038/s42005-025-02324-6.

Correspondence and requests for materials should be addressed to Lac Nguyen or Mohammad-Ali Miri.

Peer review information *Communications Physics* thanks the anonymous reviewers for their contribution to the peer review of this work.